System and machine learning-guided materials design for high-pressure hydrogen compression

Matthew D. Witman[1,*], Brendan C. Davis[1], Vitalie Stavila[1,^], and Terry Johnson[1,†]

[1]Sandia National Laboratories, Livermore, CA 94551, USA

[*]*mwitman@sandia.gov*; [^]*vnstavi@sandia.gov*; [†]*tajohns@sandia.gov*

Abstract

Cost effective and reliable hydrogen compression remains a challenging barrier in the wide-spread adoption of hydrogen as an energy carrier. The prevailing technology of mechanical compression suffers from several drawbacks, some of which can be addressed by non-mechanical compression strategies (e.g., electrochemical or metal hydride-based thermal compression). Thermally driven metal hydride compression strategies typically rely on multi-stage metal hydride-based compressors; however, discovering or optimizing low-stability metal hydrides that can pressurize hydrogen upwards of 1000 bar is difficult, both with respect to computational predictions and experimental validation. Here we (1) demonstrate that simple machine learning-derived design rules can inform rational design of alloying strategies yielding low-stability hydrides, (2) validate their experimental pressure-composition-temperature (PCT) isotherms up to 875 bar, and (3) utilize a dynamic systems-level model of a metal hydride compressor design to evaluate their performance under realistic operating conditions. Importantly, this analysis yields predicted operational efficiencies of both 2-stage (90-875 bar) and 3-stage (20-875 bar) metal hydride compressors to enable further evaluation of this technology and its techno-economic outlook.

Keywords: Metal Hydrides; Hydrogen Compression; Machine Learning; System Modeling; Alloy Optimization

Introduction

Hydrogen is an energy carrier that presents distinctive opportunities to advance a variety of technologies, due to its notable gravimetric energy density of $120\,\mathrm{MJ\,kg^{-1}}$ and versatile end uses in combustion, in fuel cells, as a chemical reductant, etc.[1] Currently, most hydrogen is produced from Steam Methane Reforming (SMR), which involves reacting natural gas with steam.[2] Additionally, other fossil fuel-based methods, such as coal gasification, can also be employed to produce hydrogen, as the demand for hydrogen increases.[3] Hydrogen also displays considerable potential for production through renewable energy sources[4] or via the direct mining of natural hydrogen.[5] Regardless of the production method employed, hydrogen is usually generated as a gas at relatively low pressures ranging from 1 to 50 bar, necessitating additional compression for effective storage and transportation.[6] While mechanical compressors, including piston and diaphragm types, are commonly employed, they exhibit limitations such as high operating costs and limited reliability. In addition, the complex designs of most mechanical compressors suffer from hydrogen leakage, produce significant noise during operation, and lead to increased maintenance requirements.[7]

New technologies focused on metal hydrides for hydrogen compression are being developed, utilizing the reversible reaction between metal alloys and hydrogen at various pressures. These compressors offer several advantages, including high discharge pressures of up to 1000 bar H_2, excellent scalability, and a modular design that allows the use of low-grade thermal energy to enhance energy efficiency.[7] The absence of moving parts simplifies their design, increases reliability, and reduces noise, making them an attractive option for hydrogen compression. Metal alloys based on AB, AB2, or AB5 phases are typically considered as active materials for the development of single-stage and multi-stage hydride compressors.[8–10] However, as noted by Lototskyy et al.[8] and Yartys et al.,[9] only a limited number of interstitial-type metal hydrides possess the necessary reversibility and reaction kinetics to be effective in these applications. In addition, the pressure-composition-temperature (PCT) curves of many alloys proposed for H_2 compression exhibit sloped plateaus and significant absorption-desorption hysteresis, which limits the usable capacity and compression ratio.[11]

Furthermore, *a priori* computational prediction and optimization of metal hydrides for high-pressure hydrogen compression is challenging for a variety of reasons. Compositional machine learning (ML) models for metal hy-

dride thermodynamic properties provide an excellent preliminary screening tool,[12–15] but highly accurate predictions for ultra-low stability hydrides remain a challenge. This primarily arises due to the imbalance of existing experimental data on which these models are trained, i.e., the extreme lack of experimental data for materials whose hydride plateaus require experimental PCT measurements greater than 100-200 bar. First-principles-based calculations or simulations enabling metal hydride phase equilibrium predictions[16,17] (i.e., PCT curves), which can themselves be accelerated by various machine-learning approaches,[18,19] have been proposed as well and can in principle overcome out-of-distribution accuracy issues, but these typically cannot account for sloping plateaus and hysteresis which also substantially impact a metal hydride's compression performance; therefore, experimental validation is required anyway, requiring highly specialized experimental equipment for accurate PCT measurements up to 1000 bar.

In this work we leverage metal hydride thermodynamic design rules, derived from explainability analysis of compositional ML models, to propose substitution strategies to fine-tune an existing and already promising materials' hydriding thermodynamics for high-pressure compression applications. This approach seeks to address the relative dearth of available experimental PCT data for low-stability hydrides (hydrogen absorption/desorption above 100 bar), which is both needed to improve ML models' accuracy in this region of materials space and permit quantitative systems design studies on the efficiency and performance of metal hydride-based compressors. Upon experimentally measuring PCT curves of the fine-tuned material up to 900 bar at several temperatures, we confirm the ML predicted design rule for desorption enthalpy decrease and demonstrate the material's ability to compress 1 wt% hydrogen from ∼400 bar to ∼875 bar under a temperature swing of 20 to 150 °C. Using a comprehensive system dynamic model for a prototype metal hydride compressor[20] and the experimentally measured PCTs for this new material up to 875 bar (rather than modeled PCTs extrapolated to higher temperatures and pressures), we quantitatively predict efficiency of various multi-stage, high-pressure metal hydride compressor designs. This paves the way to further improve projected efficiencies of materials-based hydrogen compression for various use cases as we continue to further optimize this material.

Methods

Our approach to discover promising metal hydrides for hydrogen compression is schematically summarized in Figure 1, with methodology details for each step presented in the Supplementary Information (SI). Briefly, this approach starts (Step 0) by identifying alloys from the literature that already display promising PCT behavior (e.g., flat plateaus and low hysteresis), but whose thermodynamic stability is too high (i.e., plateau pressure is too low) under the temperature swing range needed for high-pressure hydrogen compression. Note that most literature PCT measurements are not performed up to ∼1000 bar, which is also needed for an assumption-free determination of compression ratio and capacity. In Step 1, we then use explainable composition-property rules derived from machine learning models to elucidate the substitution strategies likely to yield destabilization the literature alloy's hydride phase. In Step 2, we synthesize and characterize the substituted alloy and perform high-pressure PCT measurements (up to ∼1000 bar) to exactly determine compression ratio and capacity under a given temperature swing. Finally in Step 3, we utilize the high-pressure experimental PCT data as inputs to a system dynamic model of a metal hydride compressor, from which compressed H_2 flow rates, operation efficiency, etc. can be obtained.

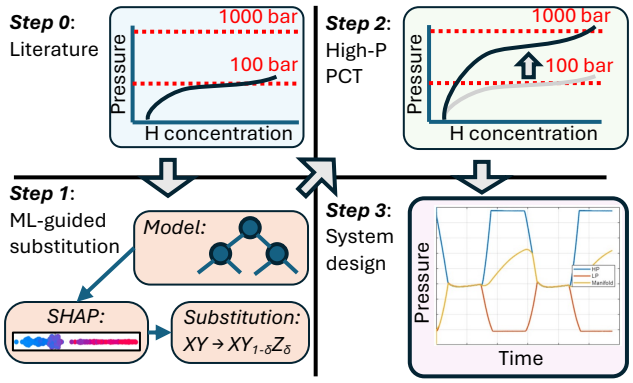

Figure 1: Schematic outlining the methodology employed in this work to identify promising alloy compositions for hydrogen compression.

Results & Discussion

Optimal materials for hydrogen compression (Step 0). The principle of hydrogen compression using a metal hydride is based on the thermodynamic relationship described by the van't Hoff equation, which correlates the equilibrium pressure of hydrogen with temperature, enthalpy, and entropy changes associated with hydride formation.[8,9] Figure 2 shows a schematic representation of hydrogen compression using a metal hydride, illustrating hydrogen absorption at a low temperature (T_L) and low pressure (P_L), followed by desorption at a higher temperature (T_H), generating an elevated pressure (P_H). At reduced temperature T_L, the metal hydride absorbs hydrogen gas at low pressure P_L to form a stable hydride phase, a process that is thermodynamically exothermic. Upon heating to temperature T_H, the chemical equilibrium shifts, favoring the endothermic desorption of hydrogen, thereby elevating the hydrogen delivery

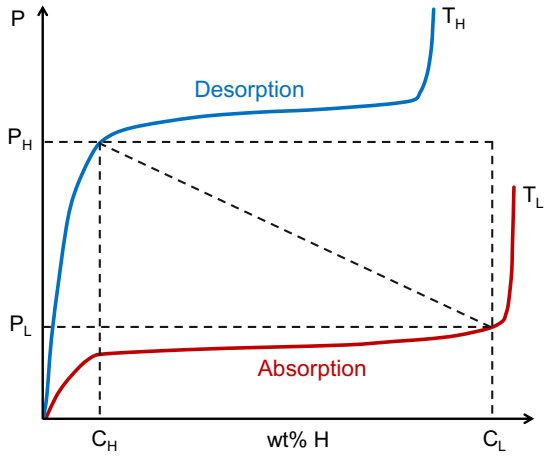

Figure 2: Schematic representation of hydrogen compression using a metal hydride. Hydrogen is absorbed at temperature T_L, H_2 pressure P_L, and concentration C_L, and desorbed upon heating at temperature T_H, generating pressure P_H with concentration C_H remaining absorbed at those conditions.

pressure P_H. The compression ratio is defined as the ratio of the high-pressure at desorption (P_H) to the low pressure at absorption (P_L).[21] This behavior underlies the functionality of metal hydride-based hydrogen compressors, where cyclic cooling and heating enable hydrogen absorption at low pressures and subsequent desorption at high-pressures. Effective thermal management, achieved through the incorporation of high-conductivity materials such as copper, aluminum, or various carbons, is imperative to facilitate rapid heat transfer and uniform temperature distribution within the hydride bed.[10,11]

Explainable ML design rules for hydride destabilization (Step 1). Compositional ML models have been widely used to predict metal hydride thermodynamic properties and subsequently screen for new or modified (high entropy) alloys with targeted thermodynamic destabilization. See the SI for more details on the ML methodology. Briefly, descriptors derived purely from a given alloy composition are generated using Magpie.[22] These features correspond to, for example, the alloy composition-weighted averages over an elemental property, $\bar{p} = \sum_i x_i p_i$ ($x_i \equiv$ atomic fraction of element i in the alloy, $p_i \equiv$ the elemental property) and serve as input to a gradient boosting regression[23] machine learning model trained to predict thermodynamic properties of Equation (1), i.e., $\ln(P^o_{eq}/P_o)$, ΔH_d, and/or ΔS_d,

$$\ln(P^o_{eq}/P_o) = -\Delta H_d/RT + \Delta S_d/R. \quad (1)$$

Here $\ln(P^o_{eq}/P_o)$ is the equilibrium plateau pressure at 25 °C with reference $P_o = 1$ bar, and ΔH_d and ΔS_d are the desorption enthalpy and entropy, respectively. However, a substantial challenge is the large imbalance of existing experimental data upon which such models are trained (e.g., the ML-ready HydPARK v0.0.6). Few van't Hoff-derived experimental data from Equation (1) exist for exceptionally low or high stability hydrides due to the difficulty of these PCT measurements, since a typical experimental apparatus is limited to pressure in the range of $10^{-3} \leftrightarrow 100$ bar and temperature in the range of $-75 \leftrightarrow 400$ °C. As shown in Figure 3b, lack of experimental data in the extrema for all target properties in turn leads to modeling predictions with increased mean absolute error (MAE) and, specifically, a systematic overestimation of stability in low stability hydrides, i.e., those with high $\ln(P^o_{eq}/P_o)$ arising from low ΔH and/or high ΔS. For materials with $\ln(P^o_{eq}/P_o) \gtrsim 6$, the test set error rapidly increases and is ∼3x larger than for materials exhibiting $\ln(P^o_{eq}/P_o)$ near ambient.

To target low-stability hydrides for potential use as a high-pressure compression material, we adopt a simple heuristic strategy, based on design rules extracted from a SHapely Additive exPlanation (SHAP) analysis,[24] rather than relying on quantitative ML prediction accuracy in these data-limited regimes. We first identify a metal hydride from the literature that already shows promise for high-pressure H_2 compression based on an appropriately low hydride stability, low hysteresis, and relatively flat PCT plateau, but whose thermodynamic stability may still not be optimal or lacks validated PCT measurement up to 1000 bar. Then, we select a substitution strategy that is consistent with the SHAP analysis (Figure 3c) design rules for tuning $\ln(P^o_{eq}/P_o)$ (or ΔH), i.e., the compositional features most likely to increase plateau pressure (by decreasing ΔH) are reducing $\bar{\nu}_{pa}$, increasing $\bar{\chi}$, decreasing $\bar{r}_c$, and increasing $\bar{\text{SG}}$#. For the set of transition metal elements E, Table 1 shows the subset of elements e that can be substituted for some target e', while satisfying an increasing number of SHAP design rules for increasing $\ln(P^o_{eq}/P_o)$.

Based on these simple heuristics, Co and Ni-substitution for Mn, Cr, or Fe tend to simultaneously satisfy the most design criteria, while substitution by Co instead of Ni will yield the largest decrease in ν_{pa} which in turn has the largest influence on ΔH and therefore $\ln(P^o_{eq}/P_o)$. Note that this SHAP analysis provides a more automated route to identifying the multi-dimensional composition-property design rules, i.e., substitution strategies, for modifying hydrides than have been historically available, where alloying design rules were empirically observed in isolation across specific subsets or classes of metal hydrides.[25–27] For example, $\bar{\text{SG}}$#'s utility as a composition-property descriptor for both ΔH and ΔS was unidentified until the use of explainable compositional ML models for metal hydride thermodynamics.[13,14]

Materials selection, synthesis, characterization, and high-pressure PCT measurements (Step 2). AB_2 alloys, particularly in the composition space of

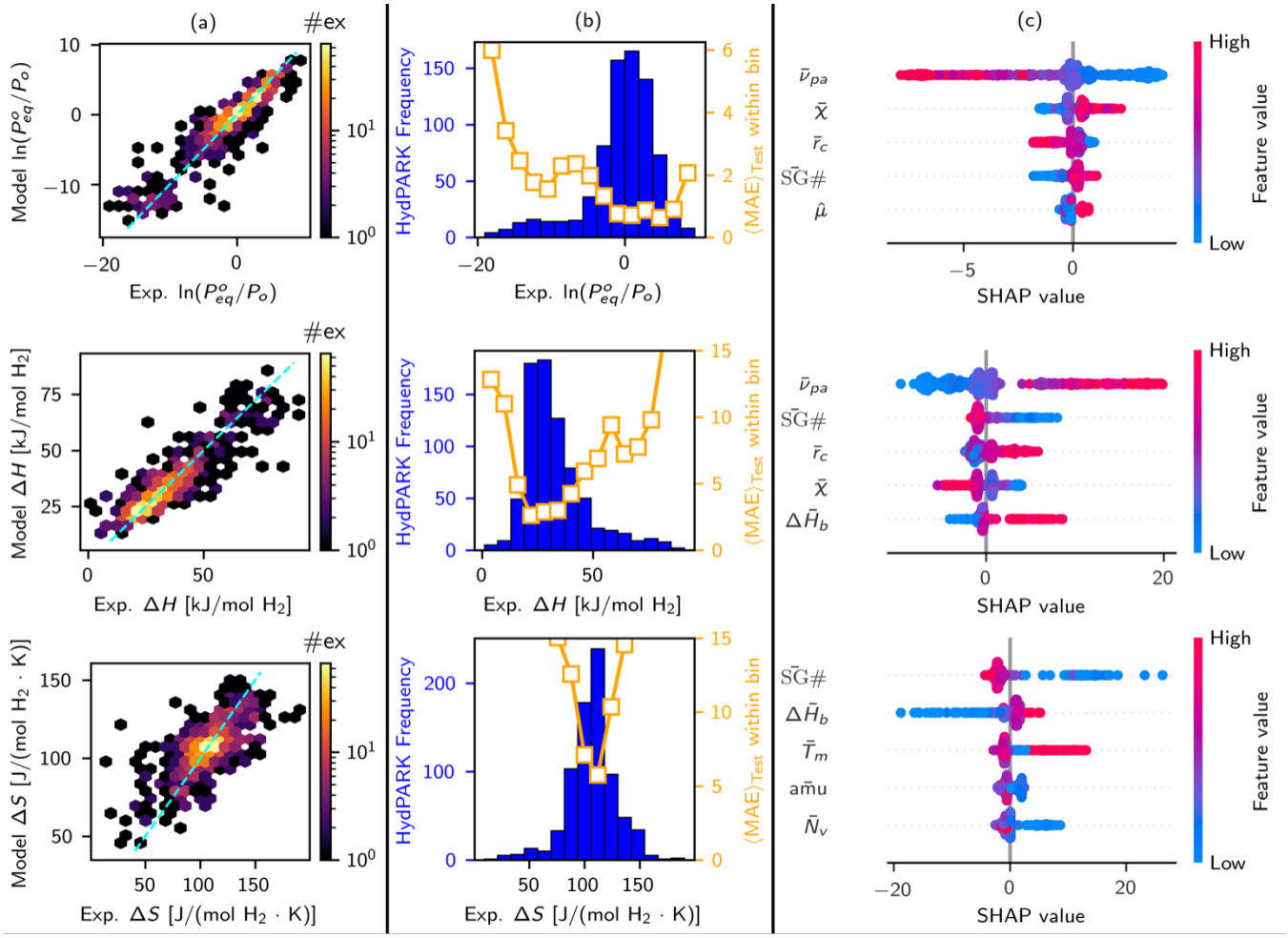

Figure 3: For target properties of $\ln(P^o_{eq}/P_o)$, ΔH, and ΔS in rows 1-3, respectively: (a) Parity plot of $K = 10$-fold test set predictions vs. experiment from a gradient boosting tree (GBT) regressor trained on v0.0.6 of the ML-ready HydPARK dataset. (b) Histogram of the underlying target property (blue) and test prediction MAE in each individual bin. (c) SHAP values for the 5 most important features for the trained GBT model. These features correspond to the following properties $p = \{\nu_{pa} \equiv$ volume per atom of the elemental solid, $\chi \equiv$ Pauling electronegativity, $r_c \equiv$ covalent radius, SG# $\equiv$ space group number of the elemental solid, $\Delta H_b \equiv$ formation enthalpy of the binary elemental hydride, $T_m \equiv$ melting temperature of the elemental solid, $N_V \equiv$ number of valence electrons$\}$.

e':	Cr	Mn	Fe	Ni
$\{\downarrow \nu_{pa}\}$	[Co,Fe,Cu,Ni,Mn]	[Co,Ni]	[Co, Mn,Ni]	[Co]
$\{\downarrow \nu_{pa}, \uparrow \chi\}$	[Co,Fe,Cu,Ni]	[Co,Ni]	[Co,Ni]	[]
$\{\downarrow \nu_{pa}, \uparrow \chi, \downarrow r_c,\}$	[Co,Fe,Cu,Ni]	[Co,Ni]	[Co,Ni]	[]
$\{\downarrow \nu_{pa}, \uparrow \chi, \downarrow r_c, \uparrow$ SG#$\}$	[]	[Ni]	[]	[]

Table 1: Possible substitution elements for select target elements, e', that are likely to destabilize the hydride phase (e.g., increase $\ln(P^o_{eq}/P_o)$) for an increasing number of SHAP design rules from Figure 3c.

$Ti(Cr, Mn, Fe)_2$, have been extensively studied as potential high-pressure compression materials since specific regions of this ternary B space can yield very large plateau pressures (e.g., $\ln(P^o_{eq}/P_o) \gtrsim 6$).[21,28,29] For example, $Ti_{1.02}Cr_{1.1}Mn_{0.3}Fe_{0.6}$ demonstrates a $\Delta H_d = 16.5\,\mathrm{kJ\,mol^{-1}}$ and $\Delta S_d = 103.8\,\mathrm{kJ\,mol^{-1}}$, maintains relatively flat plateau with small hysteresis, and exhibits faster hydrogen absorption kinetics upon small amounts of rare earth addition with minimal effect on hydride thermodynamics.[30] In the same study, a small modification to $Ti_{1.02}Cr_{1.1}Mn_{0.3}Fe_{0.6}La_{0.03}$ (hereon referred to as "base TCMFL") induced a negligible change in the thermodynamics and exhibits $\Delta H_d = 16.6\,\mathrm{kJ\,mol^{-1}}$ and $\Delta S_d = 104.2\,\mathrm{kJ\,mol^{-1}}$, while substitution with Ce or Ho instead of La yields slightly larger ΔH_d. We therefore chose TCMFL as a base material to test our ML-destabilization design rules (Table 1), choosing a small amount of Co substitution for Mn: $Ti_{1.02}Cr_{1.1}Mn_{0.2}Co_{0.1}Fe_{0.6}La_{0.03}$ (hereon referred to as "modified TCMCFL").

TCMCFL was prepared by arc-melting, followed by high-energy ball-milling to produce a fine powder. The resulting phase exhibits a C14 Laves structure (Figure 4a), with no other major crystalline phases detected. The as-milled sample was characterized using scanning electron microscopy with energy dispersive spectroscopy (SEM/EDS), revealing micron-sized particles that display a homogeneous distribution of all metallic elements present in the alloy (Figure 4b). This uniformity suggests effective mixing and milling processes during preparation. The EDS maps further indicate the presence of some oxygen in the sample, despite all precautions taken during the synthesis and handling of the alloy to minimize air exposure. A quantitative analysis of the EDS data estimates the oxygen content to be approximately 1.6 wt.%, which is common for such materials[31] and may arise from various process steps such as initial alloy synthesis, high energy ball milling, or brief air exposure during sample transfer to the SEM/EDS chamber.

A MS-16 micro reactor, manufactured by High Pressure Equipment (HiP), was loaded with 48.3 grams of the TCMCFL sample, and the reactor was coupled with a custom high-pressure PCT system capable of measurements up to approximately 1000 bar (see Supplementary Information for additional details). The reactor was leak checked, calibrated, and then the sample was activated at 200 °C in vacuum. An initial set of isotherms were measured (Figure 5a), that demonstrate the promise of this material for high-pressure compression applications. The material exhibits a reasonably flat plateau at 20 °C and minimal hysteresis, achieving an absorption capacity of 1.5 wt% at a pressure of 400 bar. Accessing the full plateau at 151 °C would exceed the pressure limitations of the PCT machine (>1000 bar), but we observe a capacity of 0.5 wt% at a desorption pressure of 875 bar. Therefore, as much as 1.0 wt% can be compressed from 400 to 875 bar via a $20 \leftrightarrow 151$ °C temperature swing. At a

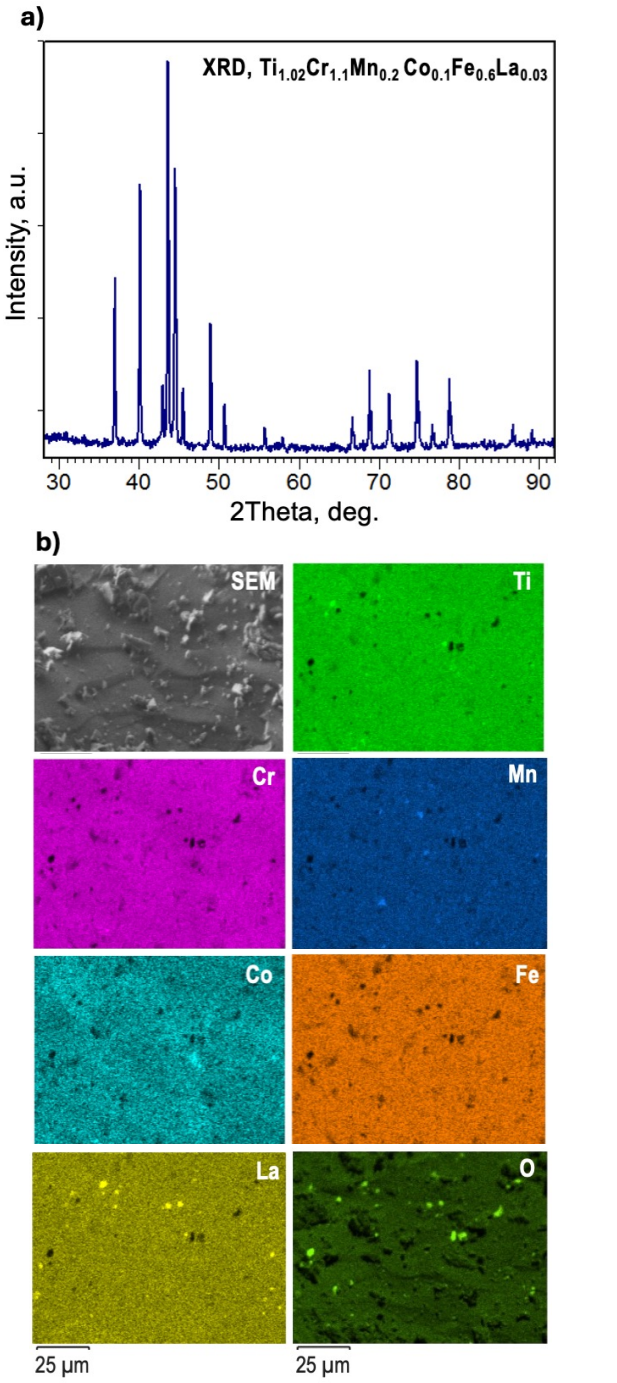

Figure 4: Experimental characterization of the TCMCFL material includes XRD of the as-milled C14 Laves phase (a), as well as SEM and EDS maps (b) confirming homogeneous elemental distributions.

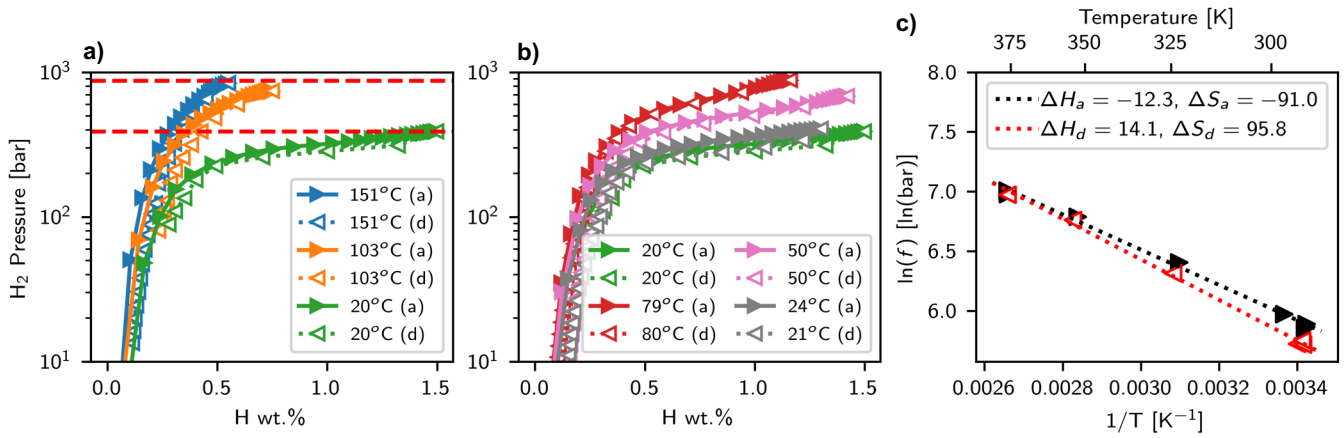

Figure 5: (a) High-pressure PCT absorption (closed markers) and desorption (open markers) for TCMCFL at three different temperatures. Dashed red lines indicate 400 bar and 875 bar. (b) Additional high-pressure PCT isotherms measurements taken 1 year after those in (a). (c) van't Hoff analysis to obtain the absorption and desorption enthalpy and entropy.

reduced desorption temperature of 103 °C, 0.7 wt% could be pressurized from 400 to 750 bar.

This material also maintains a long shelf-life under inert atmosphere, with no major change observed in the PCT isotherm after 12 months maintained under inert atmosphere. However, the more likely performance degradation pathway under practical operating conditions is air, moisture, impurity, etc. exposure and should be investigated in future work. Taken 12 months after Figure 5a, Figure 5b shows additional PCT measurements at additional temperatures for performing the van't Hoff analysis (using fugacity, f, instead of pressure[32,33]) in Figure 5c. The observed value of $\Delta H_d = 14.1\,\mathrm{kJ\,mol^{-1}}$ indeed represents a $2.5\,\mathrm{kJ\,mol^{-1}}$ decrease compared to the base TCMFL and is qualitatively consistent with the expected decrease according to the ML-derived design rules in Table 1. However, the observed value $\Delta S_d = 95.8\,\mathrm{J\,mol^{-1}\,K^{-1}}$ represents an accompanying decrease of $8.4\,\mathrm{J\,mol^{-1}\,K^{-1}}$ in the desorption entropy compared to the base TCMFL. This enthalpy-entropy compensation is common in materials design, and often limits the extent to which one can freely tune the free energy of the hydriding reaction by modulating ΔH,[18,34] as shown for this specific system in Table 2.

Table 2: ΔH_d and ΔS_d of TCMCFL (this work) vs. the materials explored in [30]. Here TCMFCe and TCMFHo represents replacement of La with Ce and Ho, respectively, in TCMFL.

Alloy	ΔH_d [kJ mol^{-1}]	ΔS_d [J mol^{-1} K^{-1}]	Source
TCMCFL	14.2	95.8	This work
TCMF	16.5	104	[30]
TCMFL	16.6	104	[30]
TCMFCe	19.3	112	[30]
TCMFHo	19.4	111	[30]

Systems-level modeling of high-pressure compressor operation (Step 3). To show the potential for the TCMCFL material in a realistic compressor application, a system-level dynamic model of a metal hydride-based compressor was used to predict 2-stage and 3-stage compressor performance using the TCMCFL hydride for the high-pressure stage. Such modeling has been performed by others[35–37] to take into account the complex process involving chemical kinetics and thermodynamics coupled with heat and mass transfer as multiple metal hydride beds undergo synchronized hydrogen absorption and desorption in a realistic system geometry. Here we use a model developed at Sandia National Laboratories using Matlab products Simulink and Simscape and described in detail elsewhere[20] and summarized in the SI.

To use the dynamic system model with measured data for candidate materials, parameterized thermodynamic models were fit using the Purdue Metal Hydride Toolbox[38] which was made available at `https://github.com/PurdueH2Lab/MetalHydrideToolbox`. The process and figures showing comparisons of each model to the measured data can be found in the SI. Four high performing materials investigated in previous work[20] were chosen for low pressure (LP) and medium pressure (MP) stages: A1=$Ti_{0.955}Zr_{0.045}V_{0.43}Fe_{0.12}Al_{0.03}Mn_{1.52}$ (known as Hydralloy C5), A2=$Ti_{0.95}Zr_{0.05}Mn_{1.55}V_{0.45}Fe_{0.09}$, A3=$TiCrMn_{0.7}Fe_{0.2}V_{0.1}$, A4=$Ti_{1.1}CrMn$). TCMCFL was chosen from the current work as the only viable high-pressure (HP) stage candidate. Several combinations of these metal hydrides, selected to best match the low- and high-temperature isotherms for the transitions between LP→MP stages and MP→HP stages, were used to predict the performance of 3-stage and 2-stage compressors

as shown in Table 3. For each design, a limited parameter study (varying source pressure, heating and cooling temperatures, and cycle time) was carried out to determine the best performance in terms of compression ratio, hydrogen flow rate at 875 bar delivery pressure, and energy efficiency (calculated as heat required per mass of hydrogen delivered). The parameters that were varied included source pressure, heating and cooling temperatures, and cycle time. Source pressure was varied between 20 and 30 bar for the 3-stage systems and 90-120 bar for the 2-stage systems, hot and cold loop temperatures were constrained to ranges of 150 to 165 °C and 10 to 20 °C, respectively, and half cycle times between 12 to 18 minutes were considered. For Design #4 in Table 3, detailed results from the dynamic system model for the 12 minute half cycle simulations with 10 °C cold loop and 160 °C hot loop temperatures are shown in Figure 6. With this design, the LP stage is filled with 90 bar to about 1.7 wt%. The HP stage is filled to 1.4 wt% as the LP stage desorbs to just under 0.8 wt%. The HP stage then produces 875 bar hydrogen while desorbing to about 0.55 wt%.

As expected, Table 3 shows the effect and importance of the relationship between the operating parameters of a metal hydride compressor. Alloy combinations must be chosen to match thermodynamics at the desired operating temperatures to maximize hydrogen flow rate and energy efficiency. For accurate predictions this must be done using realistic representations of the PCTs for each hydride that account for plateau slope and hysteresis at relevant pressures and temperatures. The study shows that tradeoffs must be made between compression ratio and energy efficiency with a larger pressure range requiring higher energy use. At some compression ratio, the number of stages must increase assuming a fixed or limited temperature range. This not only reduces energy efficiency as more heat must be used for the additional stage (sensible heating and desorption enthalpy) but also increases the capital cost of the compressor which was not considered in this study. With these effects accounted for, the study shows that the TCMCFL material enables delivery of 875 bar hydrogen at the desired flow rate, over the temperature range considered (10 - 160 °C), in either a 2-stage or 3-stage compressor configuration, depending on the source pressure.

Conclusions

Compositional machine learning models of metal hydride thermodynamics provide an excellent tool to high-throughput screen hydride thermodynamic properties for new alloy compositions,[13–15,39–42] but their performance degrades on highly out-of-distribution materials' predictions. These include ultra-low stability hydrides (e.g., those useful for high-pressure hydrogen compression), since the difficulty of PCT measurements in pressure regimes greater than 100-200 bar has led to a dearth of experimental characterization of these types of alloys. Therefore, we utilized SHAP explainability analyses of these models to obtain the composition-property design rules, and subsequent chemical substitution strategies, that are most likely to further destabilize an existing alloy's hydride phase. We used one such substitution strategy to further destabilize an already promising metal hydride for hydrogen compression, then fully synthesized, characterized, and tested TCMCFL, including high-pressure PCT measurements to confirm its ability to compress hydrogen up to 875 bar.

Using experimental PCT data as the input upon which compression cycles were designed, a system dynamic model was used to predict operational performance and efficiencies of a multi-stage metal hydride compressor using TCMCFL in the final high-pressure stage. The performance study results indicate the lower overall energy efficiency of metal hydride compressors compared to other mechanical compression technologies. This is largely unavoidable given the heat required to overcome the metal hydride reaction enthalpy and the sensible heating required to cycle the metal hydride from low to high temperature. Furthermore, despite the compression performance of TCMCFL, we were unable to design a 2-stage metal hydride system that can produce a compression ratio of 45:1 (e.g., ∼20 to 875 bar) under the temperature swing conditions of interest (10 to 160 °C).

However, the importance of energy efficiency is primarily in its relation to operating expense (OPEX). In many applications, the energy to operate the compressor must be paid for in the form of electricity and/or heat depending on the energy source. One advantage of a metal hydride compressor is that it is a heat-driven process requiring a proportionally small amount of electrical power.[43] In use-case scenarios where heat can be provided at a much lower cost than electricity, the energy usage of a metal hydride compressor may be higher than a comparable mechanical compressor but still be cost-competitive. For future work, there are clear opportunities to further optimize the TCMCFL alloy composition, since a flatter PCT plateau could simultaneously improve its working capacity and compression ratio and lead to better operational efficiencies.[7,44] Generally speaking, more advanced modeling approaches must be developed to computationally inform these compositional modification strategies. For example, while direct PCT prediction using ML-accelerated first principles calculations has been demonstrated for simpler FCC Pd alloys,[18] such approaches will need to be augmented and extended to compositionally complex AB2 alloys. *A priori* computational prediction, and therefore rational composition design, to minimize sloping plateau and hysteresis in these materials will be needed to advance future improvements of efficiency and compression ratio.

	LP	MP	HP	Half Cycle [min]	CR	P range [bar]	T range [°C]	H_2 flow rate [kg_{H_2} hr^{-1}]	Energy efficiency [kWh $kg_{H_2}^{-1}$]
1	A1	A3	TCMCML	12	29.2:1	30-875	10-150	1.1	15.5
2	A2	A4	TCMCML	12	43.8:1	20-875	10-160	1.07	17.8
3	A3	–	TCMCML	12	7.3:1	120-875	10-160	1.1	10.9
4	A4	–	TCMCML	12	9.7:1	90-875	10-160	1.05	11.5

Table 3: System-level dynamic model predictions of operational performance and efficiency of four different TCMCFL-based high-pressure hydrogen compression designs including materials selection for LP, MP, and HP stages, half cycle time, T and P operating ranges, Compression Ratio (CR), H_2 flow rate, and Energy efficiency.

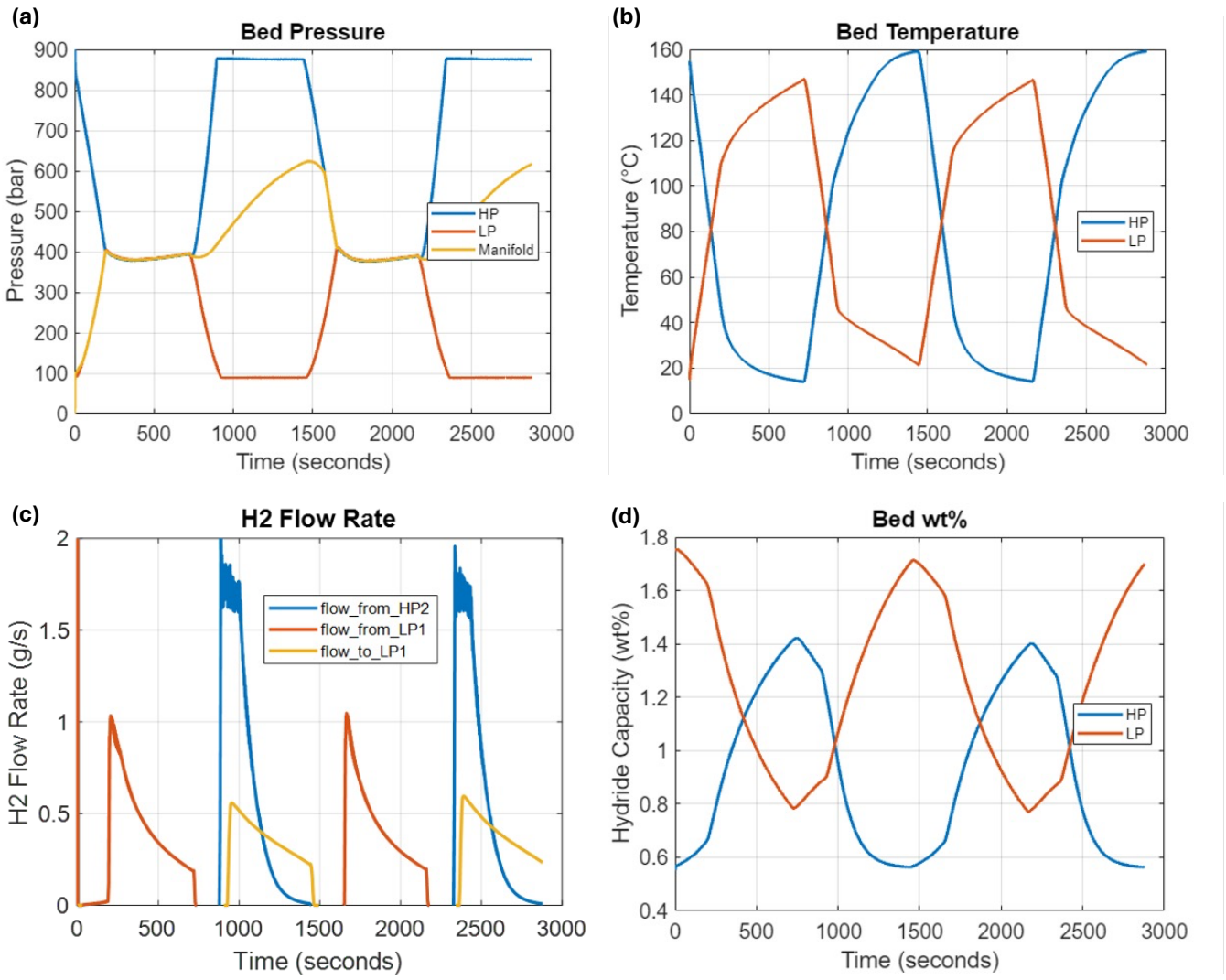

Figure 6: The dynamic system model predictions for Design #4 in Table 3, showing time-dependent operational quantities of (a) bed pressure, (b) bed temperature, (c) H_2 flow rate to/from beds, and (d) bed H wt.% for the LP and HP stages (see Supplementary Information for model description and process model diagram).

Supporting Information

Details for ML model training and validation, high-pressure PCT measurements, and system design.

Acknowledgements

The authors thank Dr. C.J. Webb for the valuable technical discussions and for the design of Figure 2. The authors gratefully acknowledge research support from the Laboratory Directed Research and Development (LDRD) program at Sandia National Laboratories. A portion of this research was supported by the Department of Energy's National Nuclear Security Administration (NNSA) under the Trilateral Framework on Cooperation in Science and Innovation among the NNSA, the Cabinet Office of Japan, and the Ministry of Science and ICT of the Republic of Korea. Sandia National Laboratories is a multimission laboratory managed and operated by National Technology & Engineering Solutions of Sandia, LLC, a wholly owned subsidiary of Honeywell International Inc., for the U.S. Department of Energy's National Nuclear Security Administration (DOE/NNSA) under contract DE-NA0003525. This written work is authored by an employee of NTESS. The employee, not NTESS, owns the right, title and interest in and to the written work and is responsible for its contents. Any subjective views or opinions that might be expressed in the written work do not necessarily represent the views of the U.S. Government. The publisher acknowledges that the U.S. Government retains a non-exclusive, paid-up, irrevocable, world-wide license to publish or reproduce the published form of this written work or allow others to do so, for U.S. Government purposes. The DOE will provide public access to results of federally sponsored research in accordance with the DOE Public Access Plan.

References

(1) Ishaq, H.; Dincer, I.; Crawford, C. A review on hydrogen production and utilization: Challenges and opportunities. *Int. J. Hydrogen Energy* **2022**, *47*, 26238–26264.

(2) Ti, W.; Ng, D. K.; Andiappan, V. Optimal integration of hydrogen production process with carbon dioxide capture, utilisation and storage. *J. Clean. Prod.* **2023**, *415*, 137697.

(3) Higman, C.; Tam, S. Advances in Coal Gasification, Hydrogenation, and Gas Treating for the Production of Chemicals and Fuels. *Chem. Rev.* **2014**, *114*, 1673–1708.

(4) Worku, A. K.; Ayele, D. W.; Deepak, D. B.; Gebreyohannes, A. Y.; Agegnehu, S. D.; Kolhe, M. L. Recent Advances and Challenges of Hydrogen Production Technologies via Renewable Energy Sources. *Advanced Energy and Sustainability Research* **2024**, *5*, 2300273.

(5) Truche, L.; Donzé, F.-V.; Goskolli, E.; Muceku, B.; Loisy, C.; Monnin, C.; Dutoit, H.; Cerepi, A. A deep reservoir for hydrogen drives intense degassing in the Bulqizë ophiolite. *Science* **2024**, *383*, 618–621.

(6) Sdanghi, G.; Maranzana, G.; Celzard, A.; Fierro, V. Review of the current technologies and performances of hydrogen compression for stationary and automotive applications. *Renew. Sustain. Energy Rev.* **2019**, *102*, 150–170.

(7) Lototskyy, M.; Linkov, V. Thermally driven hydrogen compression using metal hydrides. *Int. J. Energy Res.* **2022**, *46*, 22049–22069.

(8) Lototskyy, M.; Yartys, V.; Pollet, B.; Bowman, R. Metal hydride hydrogen compressors: A review. *Int. J. Hydrogen Energy* **2014**, *39*, 5818–5851.

(9) Yartys, V. A.; Lototskyy, M.; Linkov, V.; Grant, D.; Stuart, A.; Eriksen, J.; Denys, R.; Bowman, R. C. Metal hydride hydrogen compression: recent advances and future prospects. *Appl. Phys. A* **2016**, *122*, 415.

(10) Bellosta von Colbe, J.; Ares, J.-R.; Barale, J.; Baricco, M.; Buckley, C.; Capurso, G.; Gallandat, N.; Grant, D. M.; Guzik, M. N.; Jacob, I.; Jensen, E. H.; Jensen, T.; Jepsen, J.; Klassen, T.; Lototskyy, M. V.; Manickam, K.; Montone, A.; Puszkiel, J.; Sartori, S.; Sheppard, D. A.; Stuart, A.; Walker, G.; Webb, C. J.; Yang, H.; Yartys, V.; Züttel, A.; Dornheim, M. Application of hydrides in hydrogen storage and compression: Achievements, outlook and perspectives. *Int. J. Hydrogen Energy* **2019**, *44*, 7780–7808.

(11) Tarasov, B. P.; Bocharnikov, M. S.; Yanenko, Y. B.; Fursikov, P. V.; Lototskyy, M. V. Cycling stability of RNi5 (R = La, La+Ce) hydrides during the operation of metal hydride hydrogen compressor. *Int. J. Hydrogen Energy* **2018**, *43*, 4415–4427.

(12) Hattrick-Simpers, J. R.; Choudhary, K.; Corgnale, C. A simple constrained machine learning model for predicting high-pressure-hydrogen-compressor materials. *Mol. Syst. Des. Eng.* **2018**, *3*, 509–517.

(13) Witman, M.; Ling, S.; Grant, D. M.; Walker, G. S.; Agarwal, S.; Stavila, V.; Allendorf, M. D. Extracting an Empirical Intermetallic Hydride Design Principle from Limited Data via Interpretable Machine Learning. *J. Phys. Chem. Lett.* **2020**, *11*, 40–47.

(14) Witman, M.; Ek, G.; Ling, S.; Chames, J.; Agarwal, S.; Wong, J.; Allendorf, M. D.; Sahlberg, M.; Stavila, V. Data-Driven Discovery and Synthesis of High Entropy Alloy Hydrides with Targeted Thermodynamic Stability. *Chem. Mater.* **2021**, *33*, 4067–4076.

(15) Witman, M. D.; Ling, S.; Wadge, M.; Bouzidi, A.; Pineda-Romero, N.; Clulow, R.; Ek, G.; Chames, J. M.; Allendorf, E. J.; Agarwal, S.; Allendorf, M. D.; Walker, G. S.; Grant, D. M.; Sahlberg, M.; Zlotea, C.; Stavila, V. Towards Pareto optimal high entropy hydrides via data-driven materials discovery. *J. Mater. Chem. A* **2023**, *11*, 15878–15888.

(16) Zepon, G.; Silva, B. H.; Zlotea, C.; Botta, W. J.; Champion, Y. Thermodynamic modelling of hydrogen-multicomponent alloy systems: Calculating pressure-composition-temperature diagrams. *Acta Mater.* **2021**, *215*, 117070.

(17) Pedroso, O. A.; Botta, W. J.; Zepon, G. An open-source code to calculate pressure-composition-temperature diagrams of multicomponent alloys for hydrogen storage. *International Journal of Hydrogen Energy* **2022**, *47*, 32582–32593.

(18) Witman, M. D.; Bartelt, N. C.; Ling, S.; Guan, P.-W.; Way, L.; Allendorf, M. D.; Stavila, V. Phase Diagrams of Alloys and Their Hydrides via On-Lattice Graph Neural Networks and Limited Training Data. *J. Phys. Chem. Lett.* **2024**, *15*, 1500–1506.

(19) Guan, P.; Spataru, C.; Stavila, V.; Jones, R.; Sharma, P.; Witman, M. D. Thermodynamic modeling of complex solid solutions in the Lu-H-N system via graph neural network accelerated Monte Carlo simulations. *ChemRxiv* **2024**, 10.26434/chemrxiv–2024–6g37p.

(20) Johnson, T.; Mallow, A.; Bowman, R.; Smith, D.; Anovitz, L.; Jensen, C. *Metal Hydride Compressor for High-Pressure (875 bar) Hydrogen Delivery*; tech. rep.; Albuquerque, NM, and Livermore, CA (United States): Sandia National Laboratories (SNL), 2022.

(21) Lototskyy, M.; Davids, M.; Swanepoel, D.; Ehlers, R.; Klochko, Y.; Gizer, G.; Pasupathi, S.; Linkov, V.; Yartys, V. Development of a high-pressure 700 bar metal hydride hydrogen compressor. *J. Energy Storage* **2024**, *98*, 113072.

(22) Ward, L.; Agrawal, A.; Choudhary, A.; Wolverton, C. A general-purpose machine learning framework for predicting properties of inorganic materials. *npj Comput. Mater.* **2016**, *2*, 16028.

(23) Pedregosa, F.; Varoquaux, G.; Gramfort, A.; Michel, V.; Thirion, B.; Grisel, O.; Blondel, M.; Prettenhofer, P.; Weiss, R.; Dubourg, V.; Vanderplas, J.; Passos, A.; Cournapeau, D.; Brucher, M.; Perrot, M.; Duchesnay, É. Scikit-learn: Machine Learning in Python. *J. Mach. Learn. Res.* **2011**, *12*, 2825–2830.

(24) Lundberg, S.; Lee, S.-I. A Unified Approach to Interpreting Model Predictions. *Adv. Neural Inf. Process. Syst.* **2017**, *2017-Decem*, 4766–4775.

(25) Mal, H. V.; Buschow, K.; Miedema, A. Hydrogen absorption in LaNi5 and related compounds: Experimental observations and their explanation. *Journal of the Less Common Metals* **1974**, *35*, 65–76.

(26) Buschow, K. H. J.; Bouten, P. C. P.; Miedema, A. R. Hydrides formed from intermetallic compounds of two transition metals: a special class of ternary alloys. *Reports on Progress in Physics* **1982**, *45*, 937–1039.

(27) Yan-Bin, W.; Northwood, D. O. Calculation of the enthalpy of metal hydride formation. *Journal of the Less Common Metals* **1987**, *135*, 239–245.

(28) Charbonnier, V.; Enoki, H.; Asano, K.; Kim, H.; Sakaki, K. Improvement of hydrogenation sorption properties of Ti0.90V0.30Mn1.00Ni0.80 for ultra-high-pressure metal-hydride compressor. *Int. J. Hydrogen Energy* **2022**, *47*, 32252–32261.

(29) Charbonnier, V.; Utsumi, R.; Nakahira, Y.; Enoki, H.; Asano, K.; Kim, H.; Sato, T.; Orimo, S.; Saitoh, H.; Sakaki, K. Hydrogenation behavior of a C14 Laves phase under ultra-high hydrogen pressure. *J. Alloys Compd.* **2023**, *965*, 171348.

(30) Yao, Z.; Liu, L.; Xiao, X.; Wang, C.; Jiang, L.; Chen, L. Effect of rare earth doping on the hydrogen storage performance of Ti1.02Cr1.1Mn0.3Fe0.6 alloy for hybrid hydrogen storage application. *J. Alloys Compd.* **2018**, *731*, 524–530.

(31) Baricco, M.; Dematteis, E. M.; Barale, J.; Costamagna, M.; Sgroi, M. F.; Palumbo, M.; Rizzi, P. Hydrogen storage and handling with hydrides. *Pure and Applied Chemistry* **2024**, *96*, 511–524.

(32) Huber, M. L.; Lemmon, E. W.; Bell, I. H.; McLinden, M. O. The NIST REFPROP Database for Highly Accurate Properties of Industrially Important Fluids. *Ind. Eng. Chem. Res.* **2022**, *61*, 15449–15472.

(33) Charbonnier, V.; Enoki, H.; Asano, K.; Kim, H.; Sakaki, K. Tuning the hydrogenation properties of Ti1+Cr2-Mn laves phase compounds for high-pressure metal-hydride compressors. *Int. J. Hydrogen Energy* **2021**, *46*, 36369–36380.

(34) Allendorf, M. D.; Stavila, V.; Snider, J. L.; Witman, M.; Bowden, M. E.; Brooks, K.; Tran, B. L.; Autrey, T. Challenges to developing materials for the transport and storage of hydrogen. *Nature Chemistry* **2022**, *14*, 1214–1223.

(35) Galvis E, A.; Leardini, F.; Ares, J.; Cuevas, F.; Fernandez, J. Simulation and design of a three-stage metal hydride hydrogen compressor based on experimental thermodynamic data. *Int. J. Hydrogen Energy* **2018**, *43*, 6666–6676.

(36) Gkanas, E. I.; Khzouz, M. Numerical analysis of candidate materials for multi-stage metal hydride hydrogen compression processes. *Renew. Energy* **2017**, *111*, 484–493.

(37) Minko, K. B.; Bocharnikov, M. S.; Yanenko, Y. B.; Lototskyy, M. V.; Kolesnikov, A.; Tarasov, B. P. Numerical and experimental study of heat-and-mass transfer processes in two-stage metal hydride hydrogen compressor. *Int. J. Hydrogen Energy* **2018**, *43*, 21874–21885.

(38) Voskuilen, T. G.; Waters, E. L.; Pourpoint, T. L. A comprehensive approach for alloy selection in metal hydride thermal systems. *Int. J. Hydrogen Energy* **2014**, *39*, 13240–13254.

(39) Somo, T. R.; Lototskyy, M. V.; Davids, M. W.; Nyamsi, S. N.; Tarasov, B. P.; Pasupathi, S. Machine Learning-assisted Study of Low-, Medium-, and High-Entropy Hydrogen Storage Alloys Validated by the Experimental Data. *High Energy Chem.* **2024**, *58*, S528–S542.

(40) Strozi, R. B.; Witman, M.; Stavila, V.; Cizek, J.; Sakaki, K.; Kim, H.; Melikhova, O.; Perrière, L.; Machida, A.; Nakahira, Y.; Zepon, G.; Botta, W. J.; Zlotea, C. Elucidating Primary Degradation Mechanisms in High-Cycling-Capacity, Compositionally Tunable High-Entropy Hydrides. *ACS Appl. Mater. Interfaces* **2023**, *15*, 38412–38422.

(41) Pineda Romero, N.; Witman, M.; Harvey, K.; Stavila, V.; Nassif, V.; Elkaïm, E.; Zlotea, C. Large Destabilization of (TiVNb)-Based Hydrides via (Al, Mo) Addition: Insights from Experiments and Data-Driven Models. *ACS Appl. Energy Mater.* **2023**, *6*, 12560–12572.

(42) Agafonov, A.; Pineda-Romero, N.; Witman, M.; Nassif, V.; Vaughan, G. B.; Lei, L.; Ling, S.; Grant, D. M.; Dornheim, M.; Allendorf, M.; Stavila, V.; Zlotea, C. Destabilizing high-capacity high entropy hydrides via earth abundant substitutions: From predictions to experimental validation. *Acta Mater.* **2024**, *276*, 120086.

(43) Dashbabu, D.; Kumar, E. A.; Jain, I. Thermodynamic analysis of a metal hydride hydrogen compressor with aluminium substituted LaNi5 hydrides. *Int. J. Hydrogen Energy* **2023**, *48*, 37886–37897.

(44) Gray, E. M.; Webb, C. J. Metal-hydride hydrogen compressors for laboratory use. *J. Phys. Energy* **2020**, *2*, 034004.